Chapter 2

Atomistic Simulation: Bulk and Surface Methods

"It is only after having failed at many attempts that one succeeds in preventing the mutually attractive balls from touching."

- Charles Augustin Coulomb

The Second Electricity and Magnetism Memoir, 1785

As the number of transistors per integrated circuit persistently adheres to the exponential growth pronounced in Moore's Law [64], computers will continue to become more powerful. It is therefore now possible to model systems which were unthinkable ten years ago. For example, atomistic simulations have recently been used in the biological realm to determine complex protein structures [65]. Atomistic forces can be determined in two ways: classically (based on Newtonian mechanics) and quantum mechanically. Although this thesis predominantly deals with classical simulations, one should not disregard quantum mechanical studies which are inherently more accurate. The undesirability of quantum mechanical calculations arises when confronted with limited computing resources. Per ion modelled, classical cal-

culations are far more efficient and less computationally taxing, allowing for a larger number of atoms to be considered. Eventually, when processing power has substantially increased, quantum mechanical simulations will be much more amenable to larger systems.

The first classical atomistic simulations carried out, were those of Boswara and Lidiard who attempted to determine Schottky defect formation energies in NaCl structured alkali halides and cesium halides [66, 67]. In fact, most of the early calculations considered highly ionic and rather simple compounds. Transition metal oxides were investigated in the 1970's, using a similar methodology [68, 69]. The Harwell Laboratory was a major driving force for the continuation and progression of atomistic simulation, focusing on the calculation of basic UO_2 defect energies [70,71] as well as fission product behaviour [36, 72]. Many of the techniques pioneered in those studies are utilized in this work.

Initial atomistic simulations were limited to the calculation of bulk defect properties. Not until Tasker's code MIDAS [73], were surface properties able to be calculated. The MIDAS code, though allowing for many more types of simulation, was limited to charge neutral surfaces. The code CHAOS [74] was developed to calculate defective surface properties. As with the initial bulk calculations, initial surface calculations considered simple ionic systems, which were predominantly cubic, e.g. MgO, CaO and NiO [75, 76]. MARVIN (Minimization And Relaxation of Vacancies and Interstitials for Neutral Surfaces Program) is a more recent surface code [77], based on the fundamentals used by MIDAS and CHAOS, but updated for new potential models (to be discussed later in this chapter) and low symmetry salts such as carbonates, sulfates and phosphates. Also updated is the ability to simply introduce ions and molecules onto the surface, which was previously difficult with MIDAS.

2.1 Perfect Lattice

Ionic crystal theory can be traced back to the work of Madelung [78] and Born [79, 80]. All of the compounds considered in this thesis form ionic crystals, which is to say that they have a regular arrangement of positively charged metal atoms and negatively charged (in this case) oxygen atoms. The lattice of these materials can be described in the classical manner, which assumes all ions are formally charged and spherical and interactions between these ions obey simple central force laws. The lattice energy is therefore:

$$\mathrm{E_{lattice}} = \frac{1}{8\pi\epsilon_\circ}\left(\sum_i \sum_{j\neq i} \frac{q_i q_j}{r_{ij}}\right) + \frac{1}{2}\Phi_{\mathrm{s-r}} \tag{2.1}$$

where q_i and q_j are the charges of the ions i and j, r_{ij} is the ionic separation and ϵ_o is the permittivity of free space. The first term of Equation 2.1, the Coulombic energy, is the main interaction between ions and attracts the unlike charged ions, accounting for the major portion of the cohesive energy of ionic materials. The second term in Equation 2.1, Φ_{s-r} is the total short range interaction energy. Short range forces serve to keep the unlike charged ions from collapsing upon one another and like charged ions from becoming unbound.

The calculations carried out in this work are referred to as "static," which is to say that they do not account for lattice vibration explicitly or configurational entropy at all. Rather, the lattice energy as it appears in Equation 2.1, is calculated with the Coulombic interactions summed using a mathematical construction and the short range interactions initially summed but then neglected after a few lattice spacings. The minimum energy atomic configuration is achieved using energy minimization techniques, discussed in Section 2.1.4. This accounts for a perfect lattice. The calculation of point defect and surface energies involve further considerations,

discussed in Sections 2.2 and 2.3 respectively.

2.1.1 Ewald Summation

Despite the apparent simplicity of the Coulomb term in the equation for lattice energy, it is actually very difficult to compute, as it is a long range force. The spatial interaction of long range forces typically falls off no faster than r^{-d}, where d is the dimensionality of the system [81]. Long range interactions give rise to rather serious problems in regard to atomistic simulations, as they can span half the distance of the simulation cell. Therefore, a method to handle this problem must be introduced. The simulations used in this work make use of the Ewald summation [82].

Ewald devised a technique which sums the interactions between an ion and its periodic images. The original derivation is rather mathematically intensive. Therefore, the following treatment is a simplification which focuses on the significant aspects of the method, after an unpublished paper of Shockley and Ewald (which can be found in [83]). The lattice assumed in this description consists of spherical, non-overlapping ions, with charge of the same magnitude whether positive or negative. The total potential at a specific lattice point can be partitioned into two sub-potentials as:

$$\Psi = \Psi_1 + \Psi_2 \tag{2.2}$$

where Ψ_1 is in reciprocal space and Ψ_2 is in real space. The potential Ψ_1 is of a lattice of point charges, with a Gaussian charge distribution of equal magnitude but opposite sign superimposed on the lattice. The potential Ψ_2 is that of a lattice with a Gaussian distribution of charge fixed at each lattice point, with the same sign as the lattice. When this potential is added to Ψ_1, the overall potential is reduced to the original set of point charges. The point of splitting the overall potential Ψ into

two parts, is that a parameter η can be optimized to determine the width of the Gaussian peaks, such that both parts converge quickly and independently. Catlow and Norgett [84] determined an optimum value for this width, which is given by:

$$\eta = \sqrt[6]{\frac{N\pi^3}{V^2}} \tag{2.3}$$

where η is the width parameter, N is the total number of species and V is the unit cell volume. The charge distribution components of Ψ_1 and Ψ_2 cause the Gaussian distributions to completely drop out of Ψ, thus leaving the overall potential, Ψ, completely independent of the width parameter, η. However, the speed of convergence is dictated by this parameter.

The definition of the Madelung constant dictates that the charge distribution on the reference point is not considered to contribute. In other words, ions do not feel their own electrostatic potential. Therefore, Ψ_1 can be expressed as the difference:

$$\Psi_1 = \Psi_a - \Psi_b \tag{2.4}$$

where Ψ_a is the potential of a continuous series of Gaussian distributions of sign the same as the actual lattice and Ψ_b is the potential of a single Gaussian charge distribution on the reference ion, see Figure 2.1.

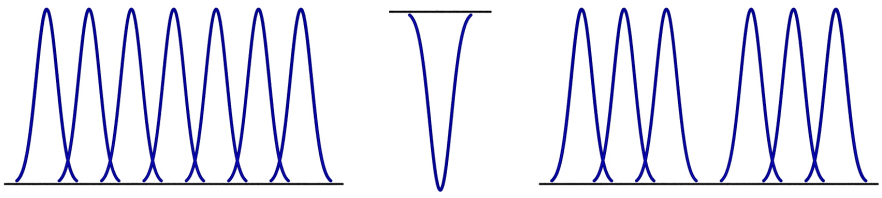

(a) Ψ_a **(b)** Ψ_b **(c)** $\Psi_1 = \Psi_a - \Psi_b$

Figure 2.1: The development of Ψ_1 from the difference of a lattice of Gaussian distributions and a Gaussian distribution at a reference point.

Ψ_a and the charge density associated with it, ρ, can be expressed in terms of a Fourier series:

$$\Psi_a = \sum_k c_k e^{i(\mathbf{k}\cdot\mathbf{r})} \tag{2.5}$$

and

$$\rho = \sum_k \rho_k e^{i(\mathbf{k}\cdot\mathbf{r})} \tag{2.6}$$

where c_k and ρ_k are coefficients and $\mathbf{k}$ is 2π times the reciprocal lattice vectors. The series converges as $\mathbf{k}$ increases and c_k and ρ_k decrease. The charge density can be related to the electrostatic potential by Poisson's equation:

$$\nabla^2 \Psi_a = -4\pi\rho \tag{2.7}$$

This relation can be used to determine an expression for Ψ_a:

$$\Psi_a = q_i \sum_j \left[q_j \frac{4\pi}{V_C} \sum_k \left(\frac{1}{k^2}\ e^{-\frac{k^2}{4\eta}} e^{i(\mathbf{k}\cdot\mathbf{r})} \right) \right] \tag{2.8}$$

where V_C is the unit cell volume. (A complete derivation of Equation 2.8 appears in Equations B.5 - 5.9 in the 1954 edition of Kittel's Introduction to Solid State Physics [83], though not in later editions, e.g. [25]).

When $\mathbf{k} = 0$, the potential Ψ_a tends to infinity. However, as it is assumed that the overall charge of a neutral unit cell is zero, the term $\mathbf{k} = 0$ can be ignored. The other constituent of Ψ_1, is the potential at the reference point due to the central Gaussian distribution:

$$\Psi_b = \int_0^\infty 4\pi r\rho\ dr = \sqrt{\frac{2q_i^2}{\epsilon_o}\left(\frac{\eta}{\pi}\right)} \tag{2.9}$$

Therefore, the difference of Equations 2.8 and 2.9 results in:

$$\Psi_1 = q_i \sum_j \left[q_j \frac{4\pi}{V_C} \sum_k \left(\frac{1}{k^2}\ e^{-\frac{k^2}{4\eta}} e^{-i(\mathbf{G}\cdot\mathbf{r})} \right) \right] - \frac{2q_i^2}{\epsilon_o}\sqrt{\frac{\eta}{\pi}} \tag{2.10}$$

The remaining part of the overall potential is Ψ_2. It is evaluated at the reference point and has three contributions from each lattice point:

$$\Psi_2 = \frac{q_i}{4\pi\epsilon_o} \sum_j \frac{q_i}{r_{ij}} \operatorname{erfc}(\sqrt{\eta}\, r_{ij}) \tag{2.11}$$

The three contributions are therefore: the point charge associated with the ion j, the Gaussian distribution contained in the sphere of radius r_{ij} at the j lattice point and the Gaussian distribution occurring outside of the same sphere, see Figure 2.2.

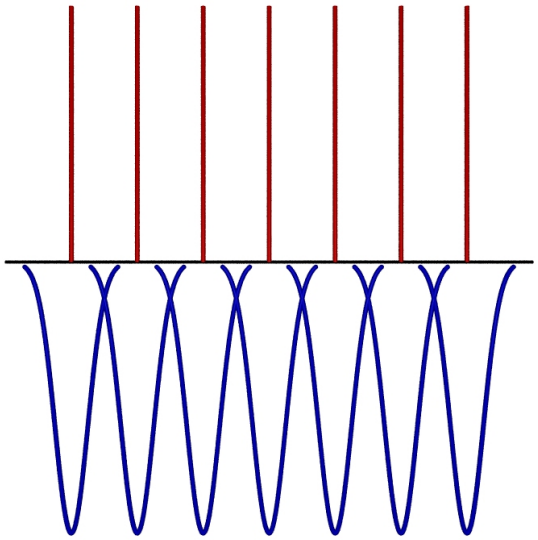

Figure 2.2: Graphical representation of Ψ_2 of the Ewald summation.

With equations for Ψ_1 and Ψ_2 determined, an expression for Equation 2.2 can be formulated, making use of Equations 2.10 and 2.11:

$$\begin{aligned}\Psi = q_i \sum_j \left[q_j \frac{4\pi}{V_C} \sum_k \left(\frac{1}{G^2}\, e^{-\frac{G^2}{4\eta}} e^{-i(\mathbf{G}\cdot\mathbf{r})} \right) \right] - \frac{2q_i^2}{\epsilon_o}\sqrt{\frac{\eta}{\pi}} \\ + \frac{q_i}{4\pi\epsilon_o} \sum_j \frac{q_i}{r_{ij}} \operatorname{erfc}(\sqrt{\eta}\, r_{ij})\end{aligned} \tag{2.12}$$

2.1.2 Short Range Potential

The Ewald sum accounts for the long range, attractive Coulomb interaction, but is unable to describe what occurs when two charged atoms are brought near one another. Equation 2.1 accounts for this short range interaction with the term Φ_{s-r}. It is important to understand how this term originates and what different forms can be adopted to describe it, as the success of this study is largely a function of the quality and moreso the accuracy with which these potentials describe this interaction.

The charge distributions of two adjacent atoms are able to overlap if they are brought near enough to one another. This causes two repulsive interactions, which if the distance between these atoms becomes sufficiently small causes the overall force between them to become repulsive, even if the ions are oppositely charged. The two terms are (a.) the Pauli term, which is a result of the Pauli exclusion principle [85,86] and (b.) the nuclear - nuclear repulsion. The generalized statement of the Pauli exclusion principle is that no two fermions can occupy the same quantum state. When electron clouds overlap (shown as charge distributions in Figure 2.3), for the Pauli exclusion principle to be satisfied, the ground state charge distribution of an electron is forced to occupy a higher energy state, thus creating an increase in electronic energy. This increase in energy gives rise to the repulsion.

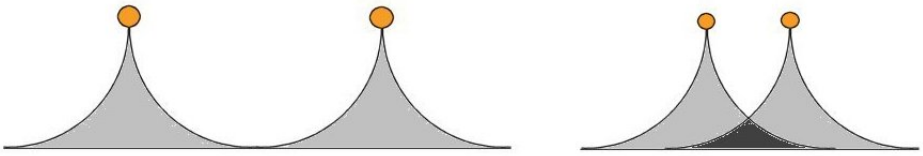

Figure 2.3: The electronic charge distribution as atoms near one another, where the orange circles denote nuclei (reproduced from [25]).

At small internuclear distances (but larger than required for the aforementioned repulsion) there also exists an attractive force, the van der Waals - London interaction. This is a relatively weak force which arises from the generation of a spontaneously induced dipole on each of the interacting species, as was postulated by Debye [87]. With the aid of quantum mechanics, London was able to determine a general expression for this attraction, where the dipole arises due to the correlated motion of electrons [88–90]. In the case of two identical atoms, this force varies proportionally to r^{-6}. Although this is a quantum mechanical effect, the r^{-6} dependency can be derived from classical electrostatics. A complete derivation for the van der Waals - London force between two hydrogen atoms can be found elsewhere [91, 92]. However, it should be noted that this force is related to the polarizability of ions. As such, it is generally not considered for cation - cation interactions, where the cations tend to be small and unpolarizable [93].

Given this broad description of the short range repulsive energy, the functional forms which can be used to describe various terms can now be explained. Equation 2.1 denotes the short range interaction as Φ_{s-r}. This term can be expanded and expressed as:

$$\Phi_{s-r} = \sum_{ij} \Phi_{ij} + \sum_{ijk} \Phi_{ijk} + \sum_{ijkl} \Phi_{ijkl} + ... \tag{2.13}$$

where ij refers to all pair interactions, ijk refers to all three body interactions, and so on. Fortunately, the work in this thesis considers only cubic, strongly ionic materials. These types of materials are relatively isotropic, thereby warranting the consideration of only pair interactions (i.e. the first term of Equation 2.13). With that established, it is now useful to discuss the various forms of the pair short range potential that have been used in other studies.

The combination of a Coulomb term with a short range repulsive term, Φ_{ij}, was

first introduced by Born and Landé [94]:

$$\Phi_{ij} = \frac{b}{r^n} \tag{2.14}$$

where b and n are constants chosen to reproduce the equilibrium interionic distance and r is the nearest distance between unlike ions. Early work using this model took $n \approx 9$. This model was later expanded when it was discovered through quantum mechanical calculations that it could not be rigorously correct (though a surprisingly good approximation, especially for very ionic materials such as the alkali halides). In an attempt to update Equation 2.14 such that it accounted for the new quantum mechanical revelations, Born and Mayer [95] introduced a short range repulsive potential of the form:

$$\Phi_{ij} = Ae^{-\frac{r}{\rho}} \tag{2.15}$$

where A and ρ are adjustable parameters. Equation 2.14 now differed from 2.15 in that Equation 2.15 contains an exponential repulsive term. At this point, Born and Mayer also added an attractive term to account for the van der Waals interaction, which, as previously mentioned, had recently been calculated [88–91]. This term took the form of C/r^6, in accord with the work by van der Waals, London and Margenau, where C is an adjustable parameter. Mayer [96] later altered this attractive term for dipole quadropole interactions, such that it took the form of D/r^8.

A combination of the repulsive term in Equation 2.14 and the C/r^6 attractive van der Waals term results in the so called Lennard-Jones potential [97–99]:

$$\Phi_{ij} = -\frac{C}{r^6} + \frac{b}{r^n} \tag{2.16}$$

where the first term represents the attractive van der Waals potential. Lennard-Jones solved for b and C for several different values for n, ranging from 9 to 14. In modern calculations, the value for n is usually 12, though the Lennard-Jones

potential is best suited to calculations concerning liquids and gases. In this work, only solids are considered, thus necessitating an alternative to the Lennard-Jones potential. If the short range repulsive term from Equation 2.15 is combined with the van der Waals attractive term, one arrives at the so called Buckingham potential (though Born and Mayer certainly deserve at least some recognition for their effort) [100]:

$$\Phi_{ij} = Ae^{-\frac{r}{\rho}} - \frac{C}{r^6} \tag{2.17}$$

where A, ρ and C are the adjustable parameters whose description of the short range interaction largely determine the success of the calculations described later in this thesis. Figure 2.4 depicts the influence of the short range potential on the overall ionic interaction. The derivation of these parameters is discussed in the following section.

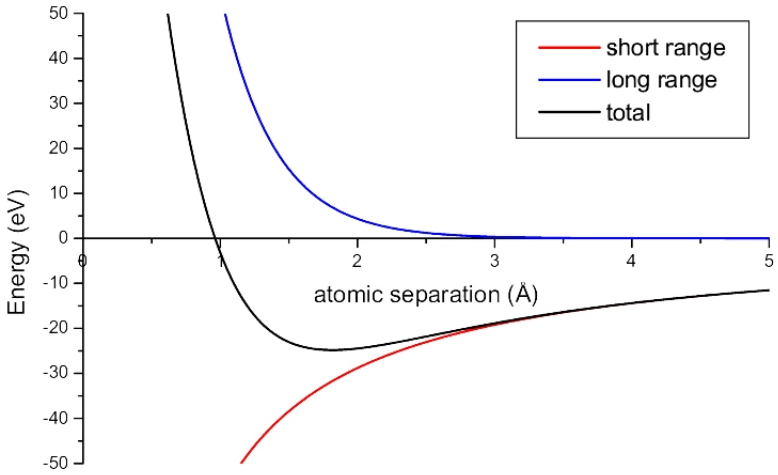

Figure 2.4: The overall potential for Sr^{2+} - O^{2-}, and its relation to the long range Coulomb interaction and short range Buckingham potential.

The short range parameters can be thought of as having loose physical meaning.

A is related the hardness of the ions, ρ describes the size of the ions while C is used to model the van der Waals interactions. This latter term can be calculated using the Slater-Kirkwood formulae [101]. The C term for identical interacting ions can be written as:

$$C_{ii} = \frac{3}{4}\alpha_i^{\frac{3}{2}} \cdot K_i^{\frac{1}{2}} \tag{2.18}$$

and for non-identical ions:

$$C_{ij} = \frac{3\alpha_i\alpha_j}{2[(\alpha_i/K_i)^{\frac{1}{2}} + (\alpha_j/K_j)^{\frac{1}{2}}]} \tag{2.19}$$

where α represents the static dipole polarizability and K is the effective electron number (i.e. the number of electrons which contribute to the polarizability). Values for α and K can be found elsewhere [102].

Short Range Potential Derivation

The success of the calculations described in this thesis depend critically upon the quality of the short range potentials. Therefore, it is essential that these terms are derived carefully in order to create an accurate description. There are essentially two principal methods of deriving potentials: empirically or by direct calculation. In this work, a combination of both methods was employed.

The empirical fitting of potentials has historically involved a reversed working of the methods described in previous sections, namely varying the short range parameters until the structural and lattice properties agree with experimental observation (as was done by Born and Landé [94]). Potentials are now chosen to reproduce a variety of properties, such as: elastic constants, high frequency and static dielectric constants and lattice energies. Any of these properties can be used in conjunction with the crystal structure for fitting. Initial values for the parameters are selected

and adjusted systematically via a least squares procedure:

$$F = \sum [f_{observed} - f_{calculated}]^2 \tag{2.20}$$

This adjustment is continued until the difference in Equation 2.20 is below a specified value. Advantages of this method include its relative simplicity as well as the ability to describe the full behaviour of a collection of atoms, including any partial covalency. However, there are several limitations of this method which need to be considered. Firstly, the crystal structure of complex oxides studied here (e.g. pyrochlores) has been determined via powder X-ray or neutron diffraction, whereas the other properties used for potential derivation (e.g elastic constants) are determined from large single crystals. Ideally, all data would come from the same crystal. If the same crystal was used, differences due to issues of chemistry (e.g. stoichiometry) would not occur. Structural data may also have inherent unreliability due to defects in the material. Furthermore, the lattice energies of these crystals are also subject to question due to the uncertainty in the second electron affinity of oxygen [103]. Harding *et al.* have closely examined the variation of the second electron affinity of oxygen with chemical composition and nuclear structure [104]. They found that assuming a single value of $\approx$ 8eV (as is usually the case) is erroneous due to this value varying with nuclear geometry and crystal structure.

A second limitation of empirical potential derivation is that only one point of the potential surface is calculated; namely, the equilibrium interionic separation. This becomes increasingly problematic when considering defective systems, as the interionic separation will shift away from the equilibrium position. To overcome the limitation of a single point interionic separation potential, parameters can be fit to a range of structures simultaneously (e.g. [105]). The resulting potentials relate to the ionic separations of several different structures, see Figure 2.5, and are therefore more *transferable* then if they were fit to a single structure.

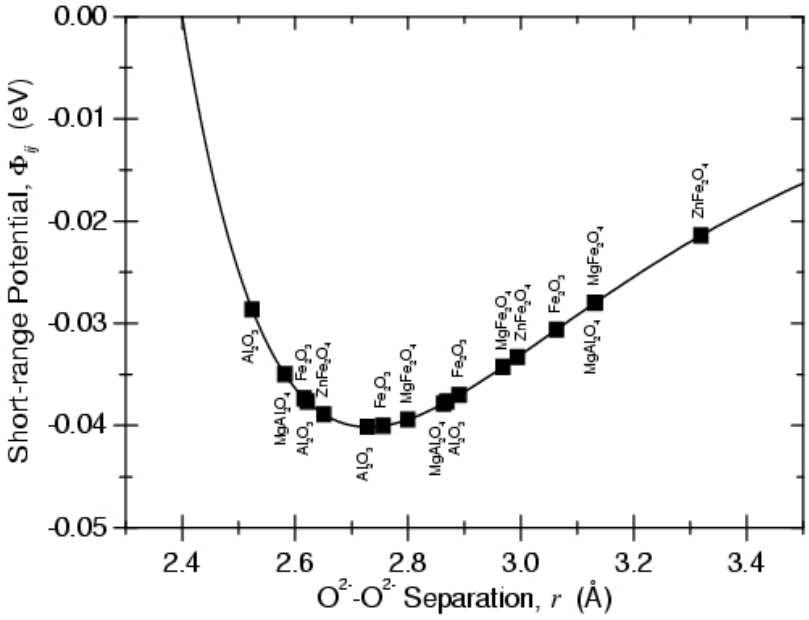

Figure 2.5: The series of compounds that the O^{2-} O^{2-} potential was fit to in order to derive this potential, reproduced from [105].

Potentials which are fit through direct calculation are derived through a number of methods, though all are based on quantum mechanics. Using techniques such as electron gas methods [106] or *ab initio* calculations [107], ionic positions are varied systematically to produce a potential energy surface that is a function of ion position. The inter ionic potential parameters are then fit to best reproduce this potential energy hyper surface.

An important point is that the potentials need to be derived in a consistent manner if they are to be used together. For example, cation - oxygen potentials describing different cations are not necessary compatible in the same simulation if they were derived with respect to different oxygen potentials. Although it may be useful to use empirical derivation and direct calculation in a concerted effort to

derive a set of potentials, it has been found that potentials obtained from different sources are generally not compatible [108].

2.1.3 Electronic Polarizability

The dielectric constant, ϵ, of a material is a measure of how effective an electric field, E, is in polarizing that material and can be expressed as:

$$\epsilon = 1 + 4\pi\frac{P}{E} = 1 + 4\pi\chi \tag{2.21}$$

where P is the polarization as defined as the dipole moment per unit volume and χ is the electric susceptibility. All of the terms in Equation 2.21 are macroscopic and easily measurable. In order to investigate microscopic phenomenon, a different property must be introduced. The *polarizability* is expressed as:

$$\alpha = \frac{p}{E_{local}} \tag{2.22}$$

where p is the dipole moment and E_{local} is the local electric field which produces the dipole. The polarizability can be thought of as a reciprocal force constant, if Equation 2.22 is rewritten as:

$$\alpha = \frac{e \cdot x}{F/e} = e^2\frac{x}{F} = e^2\frac{1}{\beta} \tag{2.23}$$

where β is the force constant of Hooke's law. As expressed in Equation 2.23, α has dimensions of volume.

In the model employed in this work, polarization is taken into account in two ways. In the first manner, ions are shifted slightly from their equilibrium positions subject to the restoring forces from adjacent ions. This is called displacement polarization. The second process involves the displacement of electrons around a fixed ion core or nucleus.

It is important to include this electronic polarizability in the methodology, especially when considering large ions and charged defects. However, including electronic polarizability increases the degrees of freedom and therefore the computational intensity. As a consequence, in this work, only anions and larger cations (e.g. Zr and Xe) are considered as polarizable in the second manner described.

To account for electronic polarizability, the shell model devised by Dick and Overhauser is employed [109]. This model describes each ion as consisting of a core of charge $X \cdot e$ and a corresponding shell of charge $Y \cdot e$, such that the total charge of the ion is $(X + Y) \cdot e$. The massless shell is coupled to the massive core by a spring of force constant k (see Figure 2.6), such that the polarizability of the free ion, α_e, can be expressed as:

$$\begin{aligned} \alpha_e &= \frac{1}{4\pi\epsilon_o}\left(\frac{Y^2}{k}\right) \\ &= 14.3994\left(\frac{Y^2}{k}\right) \end{aligned} \tag{2.24}$$

where ϵ_o is the permittivity of free space and the numerical constant applies if Y is in electron charge units and k is in units of ev·Å^2. This expression is similar to Equation 2.23, where α is in units of Å^3.

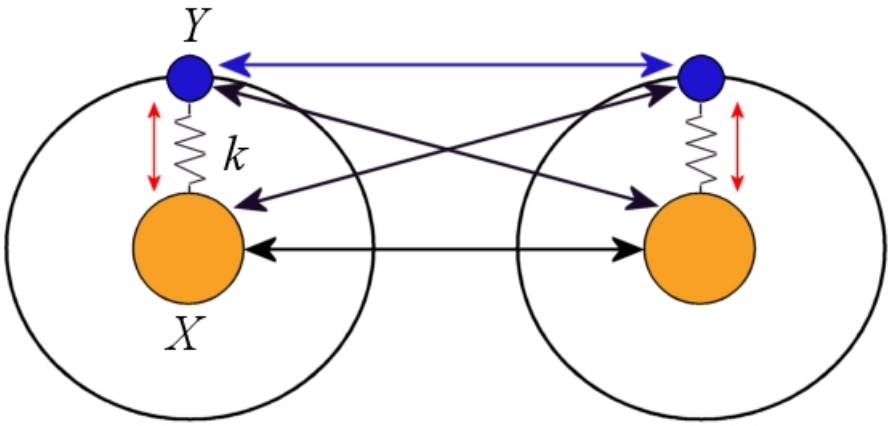

Figure 2.6: The shell model, where the orange atom is the core and the blue atom represents the charge of the massless shell. The red arrows represent polarization, black arrows represent Coulombic interactions and blue arrow represents short range interaction.

It is common for the parameters Y and k to be fit to dielectric and elastic constants. This fitting is primarily concerned with the high frequency dielectric constant, ϵ_∞, as it arises solely from the electronic polarizability, rather than having ionic polarizability contributions, as does the static dielectric constant, ϵ_s.

Although the shell model is phenomenological in nature, its use is warranted by its success in previous studies, (see for example Catlow *et al.* [110]). The strength of this model (versus other models, such as the rigid ion model or the point polarizable ion model) is that any force acting on an ion is assumed to do so via the shell, thus coupling short range interactions to the polarizability, see Figure 2.6. Clearly, this provides a framework by which it is possible to model more of the interactions occurring between species than if the shell model was not used (i.e. the rigid ion model alone).

There are however limitations to this model. First and foremost is that the shell

model does not appropriately account for the Cauchy violation [111]. If the three components of the stress tensor are given as X_1, X_2 and X_3, and the three shear components are given as X_4, X_5 and X_6, then the Hooke stress - strain relation can be expressed as:

$$X_i = \sum_{j=1}^{6} c_{ij} x_j \tag{2.25}$$

where c_{ij} are the thirty-six elastic constants. For cubic crystals, there are certain equalities:

$$c_{11} = c_{22} = c_{33}; \qquad c_{12} = c_{23} = c_{31}; \qquad c_{44} = c_{55} = c_{66}; \tag{2.26}$$

The rest of the matrix is zero if the coordinate axes and the cube axes are parallel, thus leaving only three independent components. Equivalent relations can be derived for hexagonal crystals. Even more relations can be derived if the atoms of the crystal interact with central forces (as they do in the shell model). These are the so called Cauchy-Poisson relations, for which there exist expressions for cubic and hexagonal structures. The cubic relation is as follows:

$$c_{12} = c_{44} \tag{2.27}$$

(A more thorough derivation of the Cauchy-Poisson relations can be found in Chapter II, Section 15 of Seitz's Modern Theory of Solids [112]). Unfortunately, real materials often violate Equation 2.27. For example, Table 2.1, where E is the principal Young's modulus, demonstrates that for common materials such as rocksalt and KCl, the Cauchy relation is considerably violated [113].

Material	E	c_{11}	c_{12}	c_{44}
Fluor Spar	1470	1670	457	345
Rock-salt	418	477	132	129
Potassium Chloride	372	375	198	65.5

Table 2.1: Experimental values for elastic constants demonstrating the violation of the Cauchy relation, reproduced from [113].

However, because the shell model is limited by perfect spherical symmetry, it is unable to account for this violation. Certain modifications can be made to the shell model so it is able to model the Cauchy violation. Schroder has introduced a *breathing shell*, which allows the shell to distort spherically, thus adding another degree of freedom [114]. However, this model only works for cases when $c_{12} < c_{44}$. When $c_{12} > c_{44}$, Sangster has developed a modification which allows for ellipsoidal modifications to the shell [115]. In this work, neither of these modifications have been used, but they are acknowledged as potentially useful.

2.1.4 Energy Minimization

In order for the aforementioned model to be useful in predicting perfect lattice properties, it must be combined with an energy minimization technique in order to bring the system to a state of mechanical equilibrium [116]. In this work, all ionic interactions are calculated and each ion subsequently moves a distance proportional to the force acting on the particle in the direction of the overall field. There are two procedures to minimize the lattice energy: either at constant volume or constant pressure. Constant volume minimization determines the minimum energy via ionic coordinates, where only the strains on individual ions are considered. For

constant pressure techniques, it is necessary to determine the minimum energy not only through the adjustment of ionic coordinates, but also unit cell dimensions, accounting for the strains both on individual ions as well as the unit cell.

Under constant volume conditions the lattice energy U_L can be expanded to the second order about a point r, and for the new set of coordinates r' can be expressed as:

$$U_L(r') = U_L(r) + g^T \cdot \delta + \frac{1}{2}(\delta^T \cdot \mathbf{W} \cdot \delta) \tag{2.28}$$

In Equation 2.28, g is the first derivative of the lattice energy with respect to ionic positions:

$$g = \frac{\partial U_L}{\partial r} \tag{2.29}$$

δ is the displacement (or strain) of a given ion:

$$\delta = r' - r \tag{2.30}$$

and $\mathbf{W}$ is the second derivative of the lattice energy with respect to r:

$$\mathbf{W} = \frac{\partial^2 U_L}{\partial r^2} \tag{2.31}$$

At equilibrium, the change in energy with respect to strain is zero. Therefore:

$$\frac{\partial U_L(r')}{\partial \delta} = 0 = g + \mathbf{W} \cdot \delta \tag{2.32}$$

The optimum ion displacement to give rise to the minimum lattice energy is:

$$\delta = -\mathbf{W}^{-1} \cdot g \tag{2.33}$$

or:

$$\delta = -\mathbf{H} \cdot g \tag{2.34}$$

where **H** is the Hessian matrix is the inverse of the second derivative of the lattice energy with respect to ionic displacement.

The energy of the systems considered in this work are not harmonic, thus the energy minimum can not be arrived at in a single step. Rather, subsequent displacements, in general, result in lower energy configurations. Thus, the ionic coordinates are adjusted iteratively until the forces on the atoms are zero. There are two methods of energy minimization employed in this work: Newton-Raphson and Conjugate Gradient.

All Newton-Raphson type formulae (e.g. the Borgden, Fletcher, Goldfard, Shanno formula [117]) serve to iteratively update the Hessian matrix, **H**, from Equation 2.34:

$$r_{n+1} = r_n - H_i \cdot g_i \tag{2.35}$$

This however requires the storage of the Hessian matrix of second derivatives, which is computationally intensive. Furthermore, solving for the second derivative matrix at each step would result in a less than expeditious overall calculation. For this reason, Conjugate Gradient type minimizations are also employed. These only require the calculations of the first derivatives of the lattice energy:

$$\beta = \frac{g_{i-1}^T \cdot g_{i-1}}{g_{i-2}^T \cdot g_{i-2}} \tag{2.36}$$

Conjugate Gradient calculations are computationally less expensive than those of the Newton-Raphson variety and converge quickly when far from the lattice energy minimum. However, when near the minimum, the Conjugate Gradient technique becomes less efficient due to the small gradients. Thus, a combination of these two techniques is used during the minimization process, beginning with Conjugate Gradient as a coarse refinement until a certain small gradient is met and then switching to Newton-Raphson type methods in order to finalize the minimization.

In depth mathematical discussions of energy minimization (including constant pressure minimization) can be found elsewhere [118, 119].

2.2 Defective Lattice

To paraphrase F.C. Frank, "materials are like people, it is their defects that make them interesting." Certainly the importance of defects controlling and modifying materials is clear and is the central theme of this thesis. Therefore, the model developed in the previous section to describe the perfect lattice will be expanded to account for defective systems. In this work, the method accounting for the defective lattice is based on a minimization of the total energy of a system by relaxing ions around a defect. The effect is confined to a short distance from the defect, which is facilitated by the use of a *two region* approach when calculating defect energies, see Figure 2.7. The response of the ions in the inner Region I is evaluated explicitly while the response of the ions in the outer Region II is treated as a continuum and is therefore more approximate.

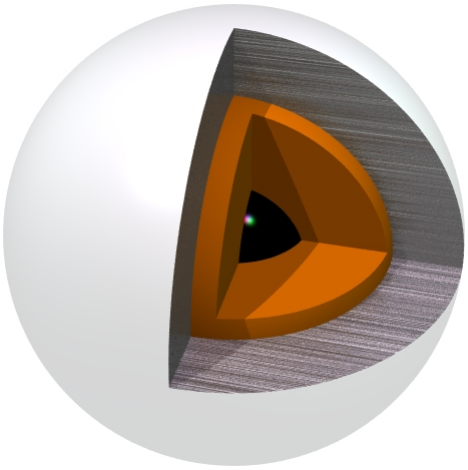

Figure 2.7: The two region approach to calculating defect energies, where the inner black sphere represents a defect, the orange sphere represents the boundary of Region I, the grey sphere Region IIa, while Region IIb tends to infinity.

Region I is a sphere of ions including the defect. The total energy of these ions is calculated explicitly as defined by the Coulombic interaction and short range potential discussed previously. The size of Region I is a very important consideration in these types of calculations. Therefore, Region I must be chosen large enough such that the defect energy converges appropriately, but computational efficiency must also be taken in to account. Figure 2.8 demonstrates the effect of Region I size on the defect energy. The Region I sizes in this thesis have been chosen to err on the side of defect energy convergence, and are found in Table 2.2.

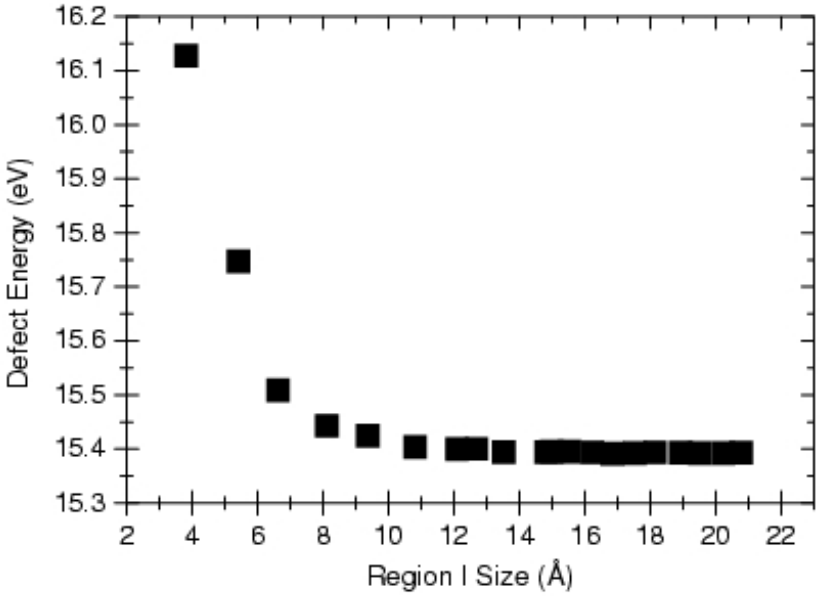

Figure 2.8: The effect of Region 1 size on defect energy, for the case of an $(V_O)^{\cdot\cdot}$ in CeO_2, reproduced from [105].

System	Region I (Å)	Region IIa (Å)
UO_2	13.67	24.06
Pyrochlores	≈10.0	≈30.0

Table 2.2: Region I and IIa radii.

Region II is subdivided into Region IIa and Region IIb. Region IIa serves as an interface between Region I and Region IIb (which extends to infinity). The changes in energy of the ions in Region IIa due to the defect and the relaxation of ions in

Region I are calculated explicitly. However, the displacements of Region IIa ions are determined in a single step by calculating the forces on these ions using the Mott-Littleton approximation [120]. This approximation is applicable since the defect is assumed to have only a small effect on the ions in Region IIb. Therefore, the entire response of Region IIb is approximated by the Mott-Littleton method.

The complication the Mott-Littleton method addresses is that the forces on any ion are not only due to the charged defect, but also to the dipoles which have been induced in the region of the lattice around the defect. This polarization can be approximately given by:

$$P = \frac{q}{4\pi r^2}\left(1 - \frac{1}{\epsilon}\right) \tag{2.37}$$

where P is the polarization, q is the charge of the defect, r is the distance from that defect and $\epsilon = \epsilon_s \epsilon_o$.

According to the conventional treatment of the defective lattice (as developed by Lidiard and Norgett [121] and Norgett [122]), the total energy of the solid containing a defect can be expressed as:

$$E = E_1(\underline{x}) + E_2(\underline{x}, \underline{\zeta}) + E_3(\underline{\zeta}) \tag{2.38}$$

where $E_1(\underline{x})$ is the energy of Region I, $E_2(\underline{x}, \underline{\zeta})$ is the energy of the interfacial Region IIa and $E_3(\underline{\zeta})$ is the energy of Region IIb. The two independent vectors $(\underline{x})$ and $(\underline{\zeta})$ are the coordinates of ions in Region I and Region II, respectively. As $E_3(\underline{\zeta})$ involves an infinite number of displacements, it can not be solved explicitly. However, if the displacements are assumed to be quasi-harmonic, it can then be defined as:

$$E_3(\underline{\zeta}) = \frac{1}{2}\underline{\zeta} \cdot \mathbf{A} \cdot \underline{\zeta} \tag{2.39}$$

where $\mathbf{A}$ is the force constant matrix. This expression can substituted into Equation 2.38 and at the equilibrium condition:

$$\frac{\partial E}{\partial \underline{\zeta}} = \left.\frac{\partial E_2(\underline{x},\underline{\zeta})}{\partial \underline{\zeta}}\right|_{\underline{\zeta}=\overline{\underline{\zeta}}} + \mathbf{A}\cdot\overline{\underline{\zeta}} = 0 \tag{2.40}$$

thus leading to an alternate expression for $E_3(\underline{\zeta})$:

$$E_3(\underline{\zeta}) = \frac{1}{2}\left.\frac{\partial E_2(\underline{x},\underline{\zeta})}{\partial \underline{\zeta}}\right|_{\underline{\zeta}=\overline{\underline{\zeta}}}\cdot\overline{\underline{\zeta}} \tag{2.41}$$

which also leads to an alternate expression for the total energy:

$$E = E_1(\underline{x}) + E_2(\underline{x},\underline{\zeta}) - \frac{1}{2}\left.\frac{\partial E_2(\underline{x},\underline{\zeta})}{\partial \underline{\zeta}}\right|_{\underline{\zeta}=\overline{\underline{\zeta}}}\cdot\overline{\underline{\zeta}} \tag{2.42}$$

where $\overline{\underline{\zeta}}$ are the equilibrium coordinates of $\underline{\zeta}$. The total defect energy can then be calculated by minimizing with respect to $\underline{x}$ and $\underline{\zeta}$.

2.3 Surface Energy Calculation

As mentioned in Chapter 1, a surface can be thought of as a large defect. Therefore, many of the previously mentioned methods can be employed when modelling surfaces. In the case of surface calculations, a unit cell is defined, cut in a specified orientation and duplicated via periodic boundary conditions in 2D, see Figure 2.9. In the third dimension the repeat block of material including the surface extending approximately 30Å in the bulk constitutes Region I. Beneath that is an additional 30Å of material, Region II, in which the ions retain their perfect lattice position. This Region II is not able to polarize in response to the surface, which, as will be seen, places an important limitation on our calculations. The interactions between ions are treated the same as when considering bulk defects, namely a long range Coulomb interaction and a short range potential. Again, the Buckingham potential has been employed when considering surfaces, as it has been for bulk materials.

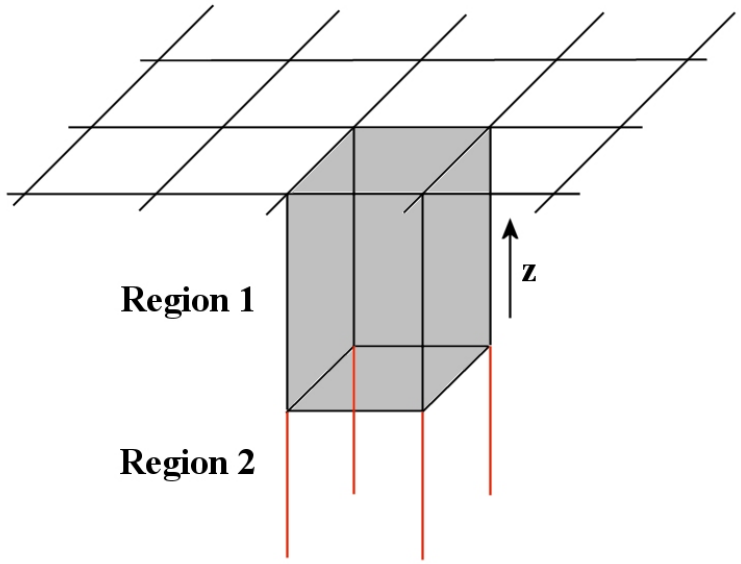

Figure 2.9: A surface simulation cell, where the z axis is normal to the surface.

A major difference in calculating surface energies and bulk defect energies is how long range electrostatic interactions between ions are computed. In the case of bulk defects, as mentioned in Section 2.1.1, the Coloumbic term of the total energy, Equation 2.1, is determined via the 3D Ewald summation. When considering surfaces, it is useful to consider this type of summation in 2D. A 2D treatment converges less quickly than the 3D surface created through slabs and gaps but the construction of 3D surfaces often results in an infinite array of dipoles which will not converge. Unfortunately, the 2D Ewald sum has a different form than the 3D. For a full description of the 2D sum, first published by Parry [123] (dutifully corrected in [124]) and Heyes [125], the reader is directed elsewhere [126].

2.4 Computational Codes

2.4.1 CASCADE

CASCADE (**C**ray **A**utomatic **S**ystem for the **Ca**lculation of **D**efect **E**nergies) was written in Fortran at the Daresbury Laboratory [127], specifically for the CRAY-1 computer. In this study, CASCADE is exclusively used for perfect lattice calculations and for defect energy calculations.

2.4.2 GULP

GULP (**G**eneral **U**tility **L**attice **P**rogram) is an improvement from earlier codes in that it has an automated empirical fitting of potential parameters feature. This feature subsequently allows for a simultaneous multi-structural fit routine.

2.4.3 MARVIN

MARVIN'S (**M**inimization **A**nd **R**elaxation of **V**acancies and **I**nterstitals for **N**eutral **S**urfaces) Program was developed at the Royal Institution of Great Britain for studying surfaces and interfaces [77]. MARVIN is based upon a similar code, MIDAS, developed by Tasker in the late 1970's [73]. MARVIN improves upon the MIDAS code by utilizing the increase in computer capability to calculate the surface energies of not only simple cubic crystals, but also more complex carbonates, sulfates, phosphates, etc. MARVIN also allows for the introduction of ions and molecules to the surface, which is important in modelling crystal growth and catalysis.

MARVIN considers a simulation cell of a finite number of atoms, which are repeated in 2D (as previously described). The cell consists of a Region I and II. In this regard, MARVIN is similar to CASCADE, in that it relaxes Region I atoms explicitly whereas those in Region II remain fixed. The total energy of the system is

defined as the energy of all the Region I structural units, all the Region II structural units and the periodic images of both regions. Since only two body terms are considered, the total energy can be expressed as:

$$E_{\text{total}} = \sum_{a}^{N_I} \left[\frac{1}{2} \sum_{l \neq 0} V_{aa}(|l|) + \frac{1}{2} \sum_{b \neq a}^{N_I} \sum_{l} V_{ab}(|r_{ab} + l|) + \sum_{b}^{N_{II}} \sum_{l} V_{ab}(|r_{ab} + l|) \right] \tag{2.43}$$

where N_I is the total number of particles in all Region I, N_{II} is the total number of all particles in Region II, l are the 2D lattice vectors and r_{ab} is the vector between particle a and particle b. The first term inside the brackets describes the interactions between a particle and its periodic images. The second term describes the interactions between all Region I particles and their images. The third terms describes the interaction between Region I and Region II.

Perfect lattice energies calculated with CASCADE can be used to determine total energies, which are subsequently used in MARVIN because both codes use energy minimization techniques and identical forces. Therefore, the energies calculated are comparable.

The MARVIN code has been used in the past to predict atomistic interaction between atomic force microscope tips and ionic surfaces [128] as well as to predict the morphology of UO_2 [45].

2.5 Listing of Short Range Potentials

Table 2.5 lists the short range Buckingham potentials used throughout this work. Shell parameters are given in Table 2.5. In each of these tables, the origination of the potential is referenced, though it should be noted that there is consistency between them as they were all derived within the Atomistic Simulation Group of

Imperial College and with respect to the same O^{2-}-O^{2-} potential.

Species	A (eV)	ρ (Å)	C (eV·Å^6)	Reference
O^{2-}-O^{2-}	9547.96	0.2192	32.0	[129–134]
Lu^{3+}-O^{2-}	1618.80	0.33849	16.27	[133, 135]
Yb^{3+}-O^{2-}	1649.80	0.3386	16.57	[105]
Er^{3+}-O^{2-}	1739.91	0.3389	17.55	[105]
Dy^{3+}-O^{2-}	1807.84	0.3393	18.77	[135]
Pr^{3+}-O^{2-}	2055.35	0.3438	23.95	[105]
Y^{3+}-O^{2-}	1766.40	0.33849	19.43	[134]
Gd^{3+}-O^{2-}	1885.75	0.3399	20.34	[105]
Eu^{3+}-O^{2-}	1925.71	0.3403	20.59	[105]
Sm^{3+}-O^{2-}	1944.44	0.3414	21.49	[105]
Nd^{3+}-O^{2-}	1995.20	0.3430	22.59	[105]
La^{3+}-O^{2-}	2088.89	0.3460	23.25	[105]
Ti^{4+}-O^{2-}	2131.04	0.3038	0.0	[136]
Ru^{4+}-O^{2-}	1215.78	0.3441	0.0	[105]
Mo^{4+}-O^{2-}	1223.97	0.3470	0.0	[105]
Sn^{4+}-O^{2-}	1414.32	0.3479	13.66	[105]
Pb^{4+}-O^{2-}	1640.34	0.3507	19.50	[105]
Zr^{4+}-O^{2-}	1502.11	0.3477	5.10	[105]
Ce^{4+}-O^{2-}	1809.68	0.3547	20.40	[137]
U^{4+}-O^{2-}	1761.78	0.3564	0.0	[138]
Ba^{2+}-O^{2-}	905.70	0.3976	0.0	[139]
Sr^{2+}-O^{2-}	682.17	0.3945	0.0	[138]
Kr^{0}-O^{2-}	800.38	0.3888	52.48	[154]
Xe^{0}-O^{2-}	598.00	0.4257	76.96	[154]
Kr^{0}-U^{4+}	5912.78	0.3191	50.34	[36]
Xe^{0}-U^{4+}	6139.16	0.3395	71.84	[36]

Table 2.3: Short-range pair potential parameters.

Species	Y (e)	k (eVÅ^{-2})	Reference
O^{2-}	-2.04	6.3	[129–134]
U^{4+}	-0.10	160.0	[129]
Zr^{4+}	-0.05	189.7	[105]
Pb^{4+}	-0.05	205.0	[105]
Ce^{4+}	-0.20	177.84	[105]
Kr^{0}	-9.90	573.7	[36]
Xe^{0}	-11.3	460.8	[36]

Table 2.4: Shell parameters.